The Greenland Ice Sheet Response to Transient Climate Change

Diandong Ren* and Rong Fu

Jackson School of Geosciences, The University of Texas at Austin, Austin, Texas

Lance M. Leslie

School of Meteorology, University of Oklahoma, Norman, Oklahoma, and Australian Sustainable Development Institute, Curtin University, Perth, Western Australia, Australia

Jianli Chen

Center for Space Research, The University of Texas at Austin, Austin, Texas

Clark R. Wilson

Jackson School of Geosciences, and Center for Space Research, The University of Texas at Austin, Austin, Texas

David J. Karoly

School of Earth Sciences, University of Melbourne, Melbourne, Victoria, Australia

ABSTRACT

This study applies a multiphase, multiple-rheology, scalable, and extensible geofluid model to the Greenland Ice Sheet (GrIS). The model is driven by monthly atmospheric forcing from global climate model simulations. Novel features of the model, referred to as the scalable and extensible geofluid modeling system (SEGMENT-Ice), include using the full Navier–Stokes equations to account for nonlocal dynamic balance and its influence on ice flow, and a granular sliding layer between the bottom ice layer and the lithosphere layer to provide a mechanism for possible large-scale surges in a warmer future climate (granular basal layer is for certain specific regions, though). Monthly climate of SEGMENT-Ice allows an investigation of detailed features such as seasonal melt area extent (SME) over Greenland. The model reproduced reasonably well the annual maximum SME and total ice mass lost rate when compared observations from the Special Sensing Microwave Imager (SSM/I) and Gravity Recovery and Climate Experiment (GRACE) over the past few decades.

The SEGMENT-Ice simulations are driven by projections from two relatively high-resolution climate models, the NCAR Community Climate System Model, version 3 (CCSM3) and the Model for Interdisciplinary Research on Climate 3.2, high-resolution version [MIROC3.2(hires)], under a realistic twenty-first-century greenhouse gas emission scenario. They suggest that the surface flow would be enhanced over the entire GrIS owing to a reduction of ice viscosity as the temperature increases, despite the small change in the ice surface topography over the interior of Greenland. With increased surface flow speed, strain heating induces more rapid heating in the ice at levels deeper than due to diffusion alone. Basal sliding, especially for granular sediments, provides an efficient mechanism for fast-glacier acceleration and enhanced mass loss. This mechanism, absent from other models, provides a rapid dynamic response to climate change. Net mass loss estimates from the new model should reach $\sim$220 km^3 yr^{-1} by 2100, significantly higher than estimates by the Intergovernmental Panel on Climate Change (IPCC) Assessment Report 4 (AR4) of $\sim$50–100 km^3 yr^{-1}. By 2100, the perennial frozen surface area decreases up to $\sim$60%, to $\sim$7 $\times$ 10^5 km^2, indicating a massive expansion of the ablation zone. Ice mass change patterns, particularly along the periphery, are very similar between the two climate models.

---

* Current affiliation: Australian Sustainable Development Institute, Curtin University, Perth, Western Australia, Australia.

Corresponding author address: Dr. Diandong Ren, Australian Sustainable Development Institute, Curtin University, Perth WA 6845, Australia.
E-mail: diandongren1972@mail.utexas.edu.

1. Introduction

The Greenland Ice Sheet (GrIS), because of its large size, unique location, and strong thermal contrast with adjacent open waters, has a strong influence on large-scale atmospheric variations (Wallace 2000; Bromwich et al. 1999), and its melting has a potential influence on global sea level rise (Yin et al. 2009). Its response to a warming climate and the resultant influence on global and regional climate is widely acknowledged (Thomas 2001; Steffen and Box 2001). Compared with Antarctica, the GrIS has a faster mass turnover. Marine-terminating glacier calving, together with surface and basal melting from fast-glaciers at the periphery of the GrIS, drain large volumes of ice. Recent findings indicate that glacier–ocean interaction also played an important role in the recent acceleration of the outlet glaciers of Greenland (Straneo et al. 2010; Rignot et al. 2010). Discharge rates are determined largely by fast-glacier dynamics, which presently are poorly understood (Abdalati and Steffen 2001) and inadequately represented in previous ice dynamics models.

Remote sensing measurements (Krabill et al. 2000; Abdalati and Steffen 2001; Rignot and Kanagaratnam 2006) have revealed increased flow speeds, widespread melting of the ice surface, and accelerating mass loss from peripheral outlet glaciers. These observations suggest that ice mass loss has accelerated in the last decade, with ice flow speeds significantly higher than previously estimated.

Ice core data during glacial periods from Summit of the GrIS indicate that temperature and accumulation rates can increase significantly over periods ranging from years to decades (Alley 1993), suggesting that observed melting could be influenced by large natural variability on interannual to decadal scales, in addition to rapid surface temperature warming caused by anthropogenic forcing.

The response of the GrIS to climate change has been investigated in sensitivity studies (e.g., Kuhn 1981; Ambach 1985) using idealized future atmospheric conditions, paleoclimate scenarios (Huybrechts et al. 1991; Van de Wal and Oerlemans 1997; Greve 2000), or temperature and precipitation rates derived from climate models (Ohmura et al. 1996). For example, the Intergovernmental Panel on Climate Change (IPCC) Assessment Report 4 (AR4), using a simple surface mass balance estimation for sea level predictions, states that "quantitative projections of how much the accelerated ice flow would add (to sea level rise) cannot be made with confidence, owing to limited understanding of the relevant processes (FAQ Section 5.1)."

Here we introduce an ice sheet dynamics model, the scalable and extensible geofluid modeling system (SEGMENT-Ice), which is driven by monthly surface meteorological conditions provided by two relatively high-resolution coupled general circulation models (CGCMs) that participated in the IPCC AR4 (Hegerl et al. 2007). A key new feature of the ice dynamics model is a granular sliding layer between the bottom ice layer and the lithosphere layer. The treatment is based on recent developments in granular material rheology (Jop et al. 2006). Because a lubricating layer of basal sediments present between the ice and the bedrock enhances ice flow. A lubricating layer of basal sediments that is present between the ice and the bedrock enhances the ice flow and is a mechanism for large scale surges (MacAyeal 1992; Alley et al. 2006) in a warming future world. SEGMENT-Ice was validated against satellite observations of total ice mass loss, surface melting area and elevation changes over Greenland in the recent decade. The model then is used to determine future mass loss and ice flow by the middle and end of the twenty-first century using CGCM simulations under the A1B scenario from the IPCC Special Report on Emissions Scenarios (Nakicenovic and Swart 2000).

2. Data and methods

a. Digital elevation map, geothermal heat flux, and initial ice temperature field

We use the surface topography [digital elevation map (DEM)] and bedrock topography provided by Bamber et al. (2001). The surface DEM is used to calculate strain, stress, and surface slope. The latter in turn is used to estimate the meltwater redistribution. We use the original 5-km resolution of ice thickness and DEMs. The total ice volume is 2.89×10^6 km^3, close to the estimate of 2.81×10^6 km^3 from Weng (1995), but significantly larger than a previously quoted value (Ohmura et al. 1996; Weidick 1995) of 2.6×10^6 km^3.

In situ measurements of ice profile temperatures are very limited over Greenland. Therefore, we use the initial temperature field from a paleoclimate simulation of the Simulation Code for Polythermal Ice Sheets (SICOPOLIS; Greve 2000), which covers the entire last glacial–interglacial cycle (150-kyr BP; Greve 2005), to initialize the model. The ice sheet temperature regime is controlled by both the surface energy balance history and the spatial distribution of geothermal heat flux (Greve 2005; Cuffey et al. 1995; Pollack et al. 1993). For future simulations, we hold the geothermal pattern constant as in the hf_pmod2 experiment of Greve (2005) because it provides a realistic representation of current Greenland ice sheet geometry and flow fields.

b. GRACE and IceSAT datasets

The Gravity Recovery and Climate Experiment (GRACE) satellite mission data are used to estimate ice

mass changes over Greenland (Chen et al. 2006). Monthly gravity data are used from the Center for Space Research GRACE release 4 (CSR-RL04) to compute the total ice mass change for the period April 2002–September 2008.

The GRACE cannot provide spatial resolution finer than several hundred kilometers (Velicogna and Wahr 2006), preventing the evaluation of detailed spatial features simulated by the ice model using the GRACE data. The Geoscience Laser Altimeter System (GLAS) instrument on the Ice, Cloud, and land Elevation Satellite (ICESat) level-II GrIS altimetry data (Zwally et al. 2003) provide along-track seasonal ice sheet surface elevations. A subset of these data is used from samples that are not contaminated by thick clouds, wet snow surface, and instrument problems. First, we average the pixels of years 2003 and 2007 into 5-km boxes and then compare the maps from these two years to determine ice sheet elevation changes.

c. Climate model output

The horizontal model resolution improves the regional simulation of precipitation (Genthon 1994) and, for Greenland, may lead to overestimation of precipitation (Ohmura et al. 1996). Thus, two coupled general circulation models (CGCMs) with relatively fine horizontal resolutions, that is, the National Center for Atmospheric Research (NCAR) Community Climate System Model, version 3 (CCSM3) (Collins et al. 2007, ~1.4°) and Model for Interdisciplinary Research on Climate 3.2 (MIROC3.2) (Hasumi and Emori 2004, ~1.125°), were chosen. These CGCMs provide all the input variables needed by SEGMENT-Ice (Ren et al. 2007), that is, monthly-mean near surface air temperature, precipitation rate, surface (skin) temperature, surface pressure, 2-m wind speed, and all six components of radiation for determining the surface energy balance. Our estimates of the warming effects on ice sheet melting are based on the Special Report on Emissions Scenarios (SRES) A1B scenario, which assumes a balanced energy source in a future world of rapid economic growth. This scenario is chosen primarily because it reflects the most recent trends in the driving forces of emissions.

Snow accumulation timing is a critical parameter for determining ice sheet mass balance (Steffen and Box 2001). We use monthly temperature increment to determine snow accumulation anomalies and additional melting relative to the control period (the 1961–90 datum period, Ren et al. 2007) as inputs to the ice flow model, to minimize potential biases in these variables produced by climate models.

d. NCEP–NCAR reanalysis monthly means

Coupled ocean–atmospheric climate models do not resolve realistic phases for interannual and decadal climate variations. Thus, they cannot be used as climate forcing for our ice model validation against observations on interannual to decadal scales. More realistic climate forcing is provided by the National Centers for Environmental Prediction (NCEP)–NCAR reanalysis (Kalnay et al. 1996). The reanalyses are widely used by climate research community as a surrogate for real observations on large spatial scale. Reanalysis data is available only from 1948, too short a period to spin up the ice model, so we use twentieth-century simulations of the CGCMs to initialize the model, then blend in relevant atmospheric parameters from the reanalyses (http://www.cdc.noaa.gov/data/gridded/data.ncep.reanalysis.derived.surfaceflux.html), starting from 1948.

e. Ice dynamics model

The new ice model, SEGMENT-Ice, is a continuum mechanical formulation starting from a force balance model (Van der Veen 1999) and is improved by including acceleration, viscous friction, and advection terms (Ren et al. 2008). SEGMENT-Ice retains the full Navier–Stokes equations to account for nonlocal dynamic balance effects in ice flow. This differs from most previous ice dynamics models, which assume that the ice sheet is locally in dynamic equilibrium (e.g., van de Wal and Oerlemans 1994; Huybrechts 1994; Van der Veen and Whillans 1989). The thermomechanically coupled scheme is designed and implemented as one integral component of a scalable and extensible geofluid modeling system (SEGMENT; Ren et al. 2011, 2010). This model provides prognostic fields of the driving and resistive forces and describes the flow fields and the dynamic evolution of thickness profiles of the medium. The inner ice domain follows Glen's (1955) ice rheology. A granular layer is allowed between ice and unfractured bed rock. Granular viscosity parameterization is based on Jop et al. (2006). Many other ice models use only ice over bed rock configuration, whereas SEGMENT-Ice allows ice–granular material–bedrock configuration for regions with granular material presence—mostly regions with significant basal melt. Formulation of the granular law; justification of the granular layer, the omission of isostatic rebound; discussion of consistent choices of ice constitutive law and Weertman basal sliding; and new approaches in parameterizing of surface melting, runoff, and the crevasse enhancement of basal sliding are described in the appendix.

The horizontal grid spacing of the ice dynamics model is 5 km. The atmospheric parameters are downscaled to spatially match the ice geometry data, to integrate the ice dynamics model at 5-km grid spacing. There are 81 vertically stretched layers to delineate the ice thickness, including one lithosphere layer at the bottom and an adjacent granular layer. For areas with granular material

thickness less than 5 cm, the granular layer is nominal and granular rheology is not activated. The integration time step is one day, with atmospheric forcing updated every month. This temporal configuration allows an examination of surface melting extent because, for most of the surface area, melting is seasonal. The annual time step, as in most paleoclimate studies, cannot resolve this dynamic feature of melt surface area, which responds sensitively to climate warming. For ice grounded on land or extending to the sea, we apply zero-stress lateral boundary conditions. The bedrock viscosity is 8×10^{20} Pa s.

It is critical to obtain a steady flow, in agreement with the ice geometry and temperature regime, before applying the transient climate forcing to project the future state of the ice sheet. The following spinup strategy is used, starting from a zero velocity field at the given ice geometry and temperature field. Because we are dealing with full Navier–Stokes code in combination with a shear-thinning rheological law, it is important to set a suitable asymptotic viscosity for grid points with effective strain rate less than 10^{-8} s^{-1}. At present, all rheological relationships in the modeling community are based on experimental shear–strain diagrams. However, because laboratory ice mechanics experiments must be completed in a reasonable time span, it currently lacks a shear–strain diagram extending to the very small strain rate regime ($<10^{-8}$ s^{-1} also is termed an impractical slow strain rate, see, e.g., Goldsby 2006). The viscosity for those "still" grids is set to $(1 - T/T_p)^{1/5} \times 10^{14}$ Pa s, with T_p being the pressure melt temperature. As the integration continues, the effective strain rate will be greater than 10^{-8} s^{-1} and regular parameterization of the viscosity then will be activated. Depending on the detailed numerics, the exact number of integrations may vary significantly. However, the evolution is that the bottom layer reaches stability first, and then gradually the shallower layer reaches a steady state. Upon reaching a steady flow field, the dynamics and thermodynamics and the evolution of the free surface are solved in a fully thermomechanically coupled manner.

3. Model validation

The seasonal surface melting extent (SME) on the GrIS has been observed by satellites since 1979 and shows an increasing trend (see Figs. 1a and 1b, chapter 6 in Symon et al. 2005). SME is directly influenced by changing climate conditions at the ice surface and is a useful representation of the ablation zone temporal variability. The monthly integration time step in SEGMENT-Ice ice model allows estimation and validation of the summer maximum SME. Contrary to the widespread belief that melting only is related to air temperature, field experiments (L. Thompson 2007, personal communication)

demonstrate clearly that melting occurs even with air temperatures well below the freezing point. Normal ranges of the stability-dependent eddy transfer coefficient and the near-surface mean wind speed prevent a near-surface temperature of $-5°$C while net energy input for a molten ice surface remains positive (chapter 7 in Hambrey and Alean 2004). Thus, the "near-surface forcing criteria" for surface melting is stipulated in our model as a 2-m air temperature greater than $-5°$C and net radiation larger than 170 W m^{-2}. This formulation was evaluated by comparing the modeled seasonal maximum SME forced by NCEP–NCAR reanalysis with those observed by the Special Sensing Microwave Imager (SSM/I) for 1992 and 2002, respectively. In both years, the general patterns of modeled maximum SME agree well with observations (Fig. 1). In 1992, melting was confined to the narrow peripheral areas well below 2000-m elevation, except for southern and mideastern Greenland, where the melting extended close to the 2000-m elevation contour. The model reproduces this pattern with some overestimation of melting in southwest and northeast Greenland. In 2002, the maximum SME crept up to 2000-m elevation in northern Greenland and approached the 2500-m elevation in southern and mideastern Greenland. Consequently, the area of maximum SME increased from ~0.34 million in 1992 to ~0.58 million km^2 in 2002. The simulated maximum SME shows a similar pattern, although with an underestimation of the melting between the Summit and South Dome and the northeast corner of Greenland. Overall, the model realistically captures the spatial pattern and change of maximum SME for the period of 1992–2002, with a slight underestimation of the SME rate of increase.

Figure 2 compares the modeled ice surface elevations with those derived from the GLAS/ICEsat, for the period of 2002–07. Because of cloudiness, no data are available along the periphery of the ice sheet below 2000-m elevation, where much of the melting occurred. The available observations, mostly above 2000 m, show an increase of surface elevation along the central ridge, especially the Summit, of Greenland, and a decrease of elevation on the slope west of the Summit. In contrast, the model shows a small decrease in ice surface elevation along the central ridge of the GrIS, presumably because of an underestimated increase of rainfall along the narrow central ridge by the NCEP–NCAR reanalysis with coarse spatial resolution (2.5°). To the east of the Summit and over the South Dome, the model shows increased ice surface elevation, which agrees qualitatively with observations. The comparison of ice surface elevation change emphasizes the importance of high-resolution climate forcing, especially of snowfall, for realistic modeling of the ice accumulation rate.
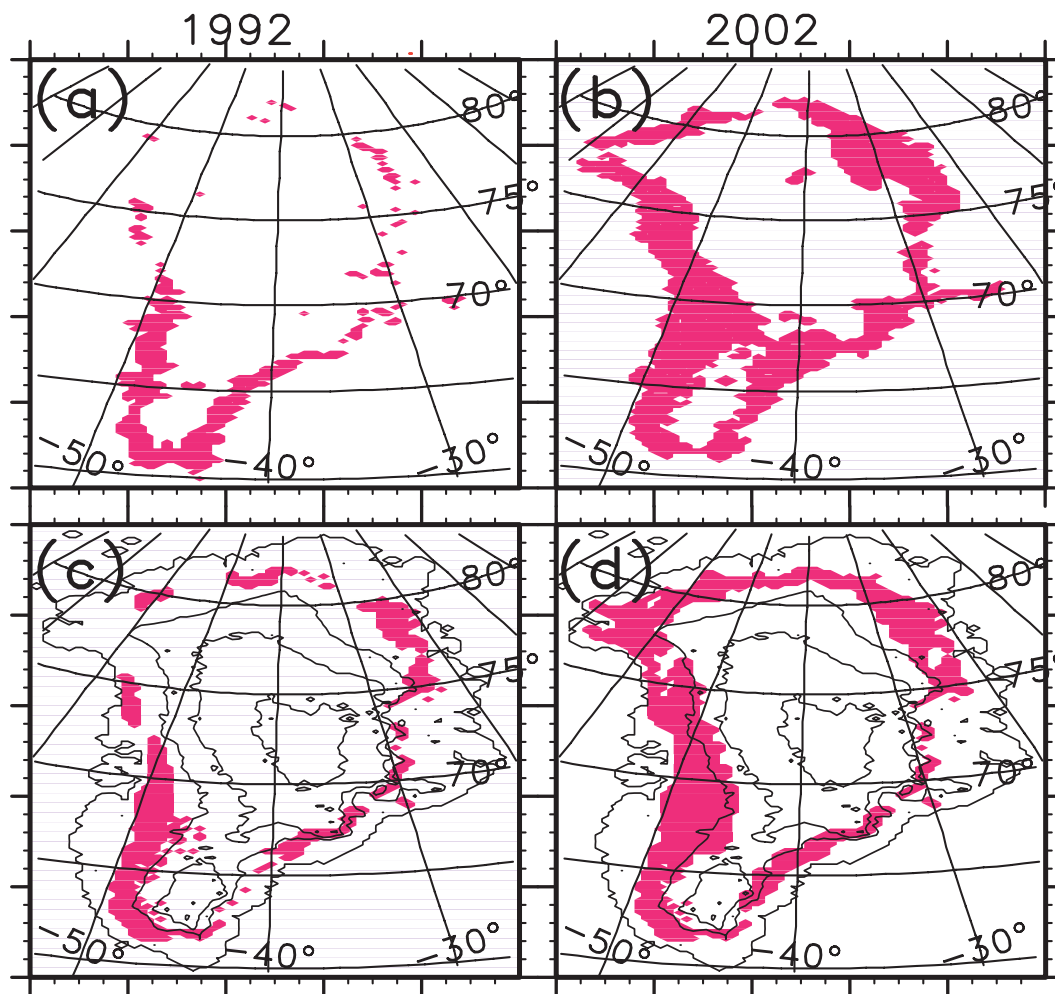
FIG. 1. (top) Observed and (bottom) simulated maximum melt surface area extent for 1992 and 2002—(a),(b) adapted from Chapter 6 in ACIA2005 and originally from Konrad Steffen, CIRES/University of Colorado at Boulder. Melting areas are in red. For (c),(d) the 2000-, 2500-, and 3000-m elevation contours also are shown.

The Fig. 3 inset compares the modeled total mass loss of the GrIS driven by the NCEP–NCAR reanalysis with that of GRACE. For the period April 2002 to September 2008, the rate of total ice mass loss agrees well between the model and observations, both showing about -147 km^3 yr^{-1} over the 2002–08 period. However, the model shows clearer and stronger seasonal cycles and interannual changes compared with those suggested by GRACE. We notice that an updated ice changing rate, covering April 2002-November 2009, is about -219 km^3 yr^{-1}, with an uncertainty level of 40 km^3 yr^{-1} (Chen et al. 2011). Compared with this series provided by the same research group, new method of leakage correction is applied based on linear projection. This new rate is closer to the model estimation.

The comparison with satellite observations of the maximum SME, ice surface elevation change, and total ice mass loss of the Greenland Ice Sheet suggest that our ice

model is able to realistically simulate spatial patterns and trends of maximum SME and of total ice mass loss over the past two decades at least, for periods when observations are available. An increase in surface elevation along the central ridge of Greenland, as suggested by the GLACE/ICEsat, is not captured by the model possibly because of the low resolution of the climate input. The seasonal and interannual variations of the total ice mass loss also are larger than those from GRACE.

4. Projected changes in Greenland Ice Sheet for the twenty-first centuries

We use the surface climate conditions provided by CCSM3 and MIROC3.2, high-resolution version [Miroc3.2(hires)], respectively, to drive the ice model and simulate the summer season melt area, ice surface
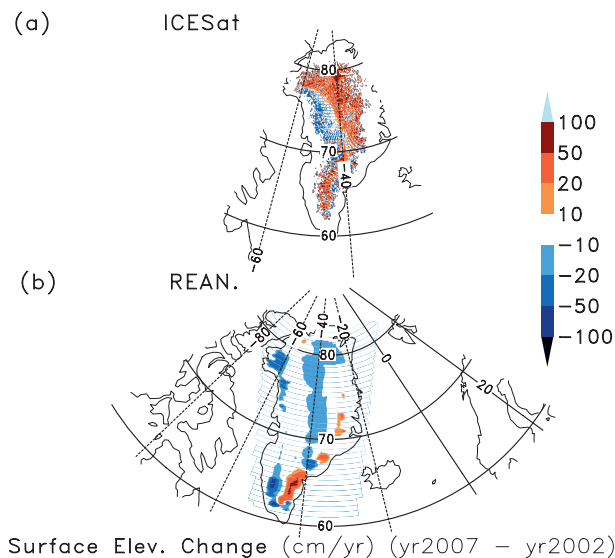
(a)　　　ICESat

(b)　　　REAN.

Surface Elev. Change (cm/yr) (yr2007 − yr2002)

FIG. 2. Elevation change rates, averaged between 2002 and 2007. The color scales are in centimeters per year. (a) For ICES at observed elevation change between 2003 and 2007, the level II (GLA06XX) data are used. Data are quality controlled by removing pixels with cloud flags > 3 and elevation flags > 32. Those white spaces are grids lacking valid data.
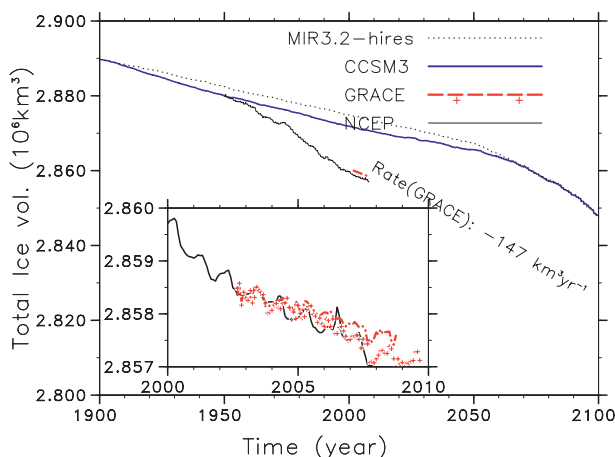

FIG. 3. Net mass balances of the Greenland ice sheet in the twentieth and twenty-first centuries. Comparisons are among using two CGCM provided meteorological conditions: MIROC3.2(hires) (dot line) and CCSM3 (solid line), NCEP reanalysis provided meteorological conditions, and GRACE observations (red dashed line). The inset is a zoom-in for the past decade. Comparisons are between model simulation using NCEP reanalysis provided meteorological conditions (black line) and GRACE measurements (red line). Because GRACE measurements are only meaningful as relative values compared with the starting point, we shifted the curve so that the two curves have the same value at the first measurement time of GRACE. We notice that an updated ice changing rate, covering April 2002–November 2009, is about -219 km^3 yr^{-1}, with an uncertainty level of 40 km^3 yr^{-1} (red cross; adapted from Chen et al. 2011).

elevations, flow pattern changes, and total mass loss of the GrIS over the twentieth and twenty-first centuries. Such an extensive simulation period is necessary because the high-latitudinal North Atlantic has significant interdecadal and multidecadal variability (Wallace 2000). It also allows an evaluation of the changes in the twentieth century and a comparison of future changes with the recent past. For brevity, we focus only on results from CCSM3 in our discussion, and show corresponding results from MIROC3.2(hires) only when there are major differences present.

For the twentieth century, we use the twentieth-century climate in coupled models (20C3M) runs (forced by observed anthropogenic and external climate forcing) of the CCSM3 and MIROC3.2(hires) to drive the ice model. For the twenty-first century, we use predicted surface climatic changes under SRES A1B scenario from these two CGCMs as inputs to the ice dynamics model.

Figure 4 shows the monthly mean surface temperatures and precipitation for the period of 1900 to 2100. The annual maximum surface temperature averaged over the GrIS lies between 270 and 275 K for the period 1990–2050 (Fig. 4a). The season with this near-freezing-point annual maximum temperature, referred to as the melting season, was confined to early June–early August period for much of the twentieth century until the 1980s. Since then, the melting season has expanded to the period of late May–mid-August by year 2000 and will expand to

the period of mid-May–early September by year 2050. For the period 2050–2100, the areal mean annual maximum surface temperature over the GrIS should rise above 275 K, well above the freezing point. The melting season also expands rapidly by 2100 to early May–late September. Figure 4c shows that the annual mean surface temperature averaged over the GrIS rises by about 6 K (CCSM3) (or 5 K, MIROC) during the twenty-first century. Modeled precipitation shows annual maxima generally during August–November, fluctuating between July and December, on decadal to multidecadal scales during the twentieth century (Fig. 4b). This rainy season is lengthened to mid-May/April of the following year during the period 2050–2100 and the annual snow precipitation rate also increases by up to 27% (Fig. 4d). Different climate models exhibit a large spread in projecting regional climate. Other CGCMs in the IPCC AR4 archive were examined for their projections of temperature and precipitation under the A1B emissions scenario. CCSM3 and MIROC3.2(hires) were chosen here as they are representative of the intermodel spread.

Because of the strong dependence of ice viscosity on temperature, it is important to obtain an accurate simulation of the temperature regime. In Fig. 5, we compare ice model simulated temperatures with corresponding
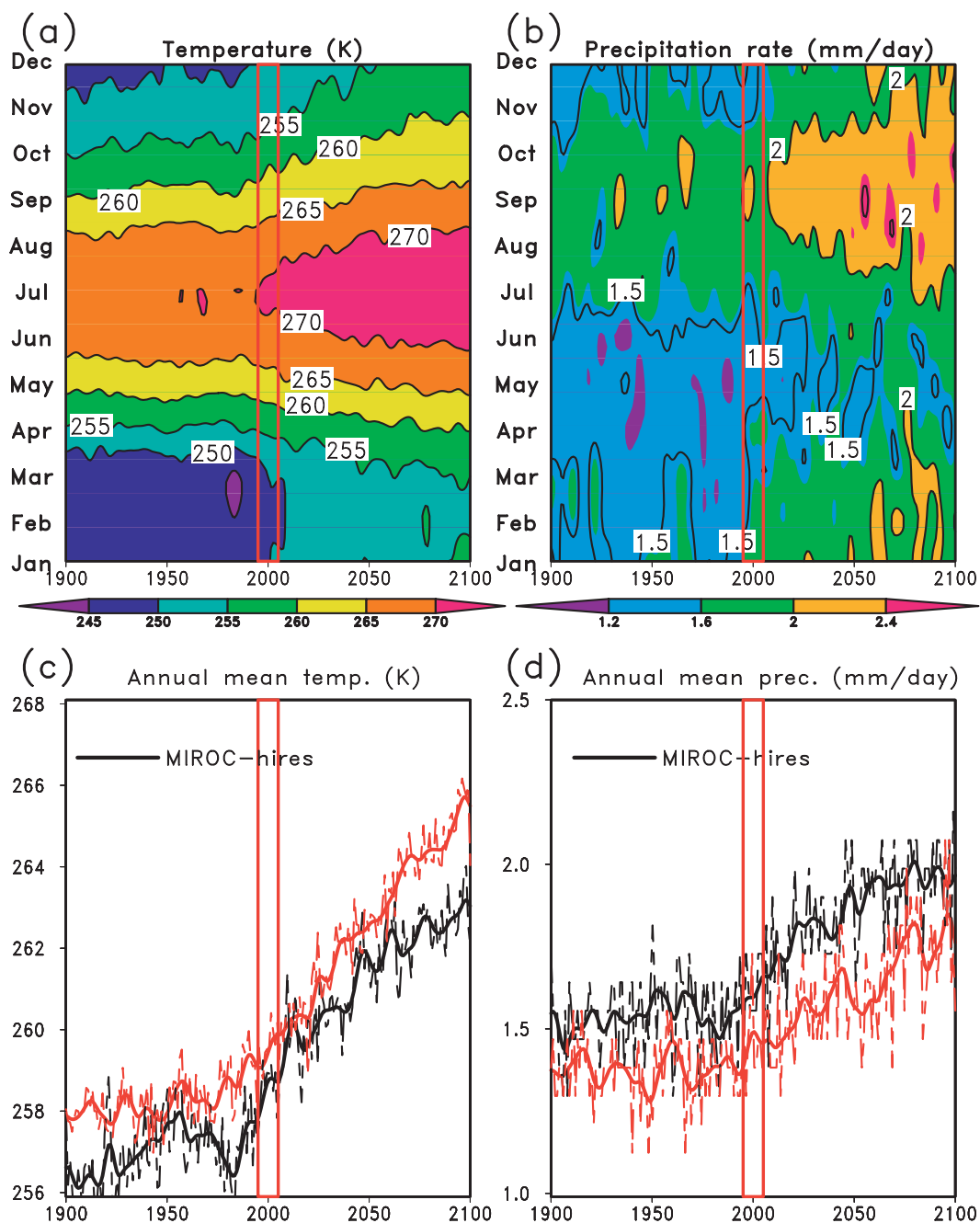
FIG. 4. Area-averaged (a),(c) temperature and (b),(d) precipitation rate over Greenland from the CCSM3 model simulation. (top) The variations in each month and (bottom) the annual-mean time series of the area-weighted (c) surface air temperature, and (d) precipitation rate. Thick curves in (c) and (d) are 21-yr low-pass-smoothed representations of the corresponding annual series. The two vertical redlines define the period corresponding to the recent survey, (a),(b) illustrate the course of annual values of month-by-month temperature/precipitation rate averaged over Greenland, putting the survey period into a long-term perspective. The (c) annual mean temperature increases by ~4°C over the next century while (d) the annual mean precipitation increases by 0.3 mm day^{-1}. The CCSM3 model time series in (c),(d) are indicated by red curve, and MIROC model time series are indicated by black curve.
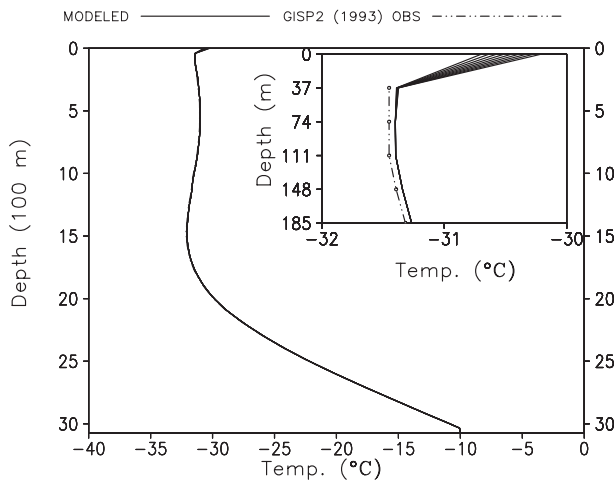
FIG. 5. Comparison of measured (dashed line) and modeled (solid lines) temperature within the ice sheet, as function of depth below surface (the thickness of the ice sheet is about 3044 m). The differences deeper than 2000 m are minimal. There are 12 monthly output profiles for year 2100. The spread (seasonality) is limited to the upper 10 m (indistinguishable at this vertical scale of display). The temperature trend in the future 100-yr period is apparent down to 1500 m, far deeper than diffusion processes can reach. The narrow warming spike at the top is due to warming of the twenty-first century.

borehole records (Cuffey et al. 1995). As the grid points of the ice model do not coincide with the borehole locations, the average value of the four nearest grids, weighted by the inverse distance from the borehole, is compared with the actual borehole observations. The initial starting temperature profile provided by the SICOPOLIS agrees well with the Greenland Ice Sheet Project 2 (GISP2) borehole observations for all depths (not shown). In the upper 1500 m, the signature from the Little Ice Age (top), the mid-Holocene warmth, and the cold glacial period (near bottom) are evident in both profiles. Starting from this initial temperature profile, our model predicts a future temperature profile at year 2100 shown in Fig. 5. The shallow warming spike at the top is due to the warming trend over the twenty-first century. For the bottom half of the ice column, the differences are generally less than 0.1°C. The shallow warming spike at the top is due to the warming trend over the twenty-first century. The temperature trend in the future 100 years reaches 1500 m, far deeper than the 35 m allowed by diffusion processes. Comparing respective contributions from different heating terms reveals that advection and diffusion terms both are an order of magnitude smaller than the strain heating term because of the enhanced surface flow speed. For the top 100 m, vertical advection contributes significantly, whereas heating deeper than 100 m is primarily due to strain heating ($\sim$10 K kyr^{-1}).

Figure 6 shows the projected maximum SME by both CGCMs. There are no permanently frozen surfaces south of 68°N (Figs. 6a and 6b). South of 75°N, the melting expands inland and approaches the 2500-m elevation contour, while on the colder northern side it generally reaches the 2000-m contour. Centered on the intersection of the 74°N and 38°W, the melt area increases steadily after 2020 and extends to $\sim$1 × 10^6 km^2 by 2100, with the melting front surpassing the 2600-m elevation contour, leaving only $\sim$7 × 10^5 km^2 of frozen surface area surrounding the summit. The two CGCMs project a very similar pattern for increased SME.

Figure 7 shows the projected change in ice surface elevation from the two CGCMs between 2060 and 2000. Despite the difference in magnitudes (MIROC3.2 produces a greater mass loss than CCSM3), both CGCMs predict strong peripheral mass loss, especially along the western peripheral area, and along the southwestern edge following the basal sliding pattern. The central portion of the ice sheet experiences little elevation change. In some regions, there is an increase in elevation because of increased wintertime snow precipitation. Snow accumulation is highest in the southeast. This region maintains its ice elevation primarily due to increased winter precipitation that offsets the increased ice flow and summertime melting. However, the net ice elevation change in this region could vary strongly on annual and decadal time scales due to changes of precipitation (Krabill et al. 2000). The ice elevation over the summit is highly stable under the future atmospheric conditions simulated by the MIROC3.2(hires) and the CCSM3.

Figure 8 shows modeled surface velocity fields for year 2000 and also the changes between 2060 and 2000. Within each ice divide (hereafter we follow the convention of Zwally and Giovinetto 2001), the flow speed increases from the central ridge toward the grounding line. For the northeastern Greenland ice stream (region II of Zwally and Giovinetto 2001) and the Jacobshavn Isbræ in central-western Greenland (the narrow convergent region along the 68°N parallel in region V of Zwally and Giovinetto 2001), our modeled surface velocity in year 2000 is close to the *European Remote Sensing-1* (*ERS-1*) satellite-observed large flow features (Fahnestock et al. 1993). The concentrated ice flow of Jacobshavn Isbræ mainly is from the ice dynamics arising from bed geometry and ice thickness profile. The formation of the northeast Greenland ice stream primarily is due to bedrock geomorphology and ice geometry and, to a lesser degree, geothermal heat flux from the bottom.

Over most of the peripheral area, the surface ice flow change is an order of magnitude greater than explainable from local elevation changes. The large change in ice flow is due to elevated temperature that reduces ice
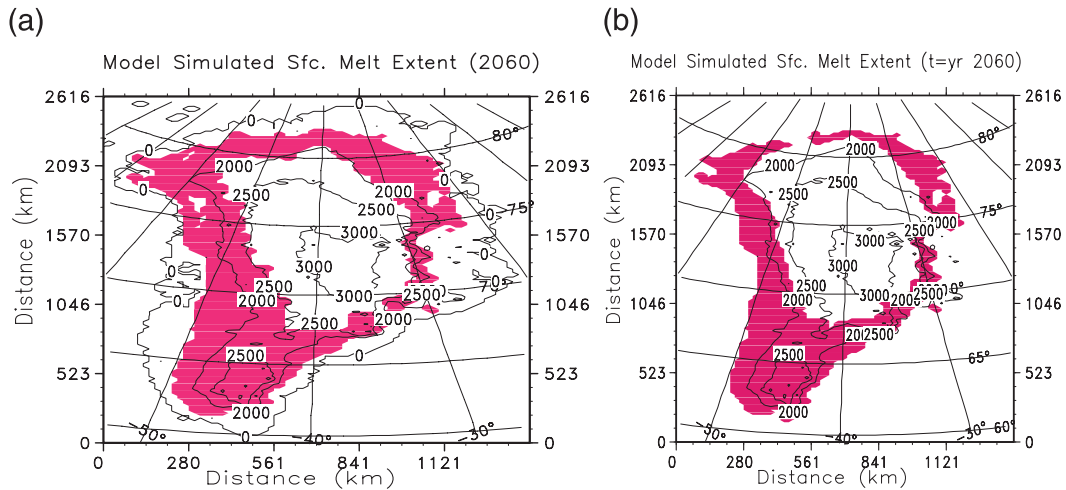
FIG. 6. Projected maximum melt surface area extent by 2060—adapted from (a) CCSM3 and (b) MIROC. Melting areas are in red. The 2000-, 2500-, and 3000-m elevation contours also are shown for location reference.

viscosity and causes nonlocal flow pattern changes. The ice thickness shrinks most for ridges in the peripheral areas because the downstream mass deficit enhances ice flow divergence. For some peripheral areas, strong surface melting (land based) and calving (extending to open waters) causes up to a 1 m yr^{-1} elevation decrease despite weaker ice flow divergence in the southwest corner of Greenland (Fig. 7).

To quantitatively compare ice flow changes between years 2000 and 2060, we plotted the u component
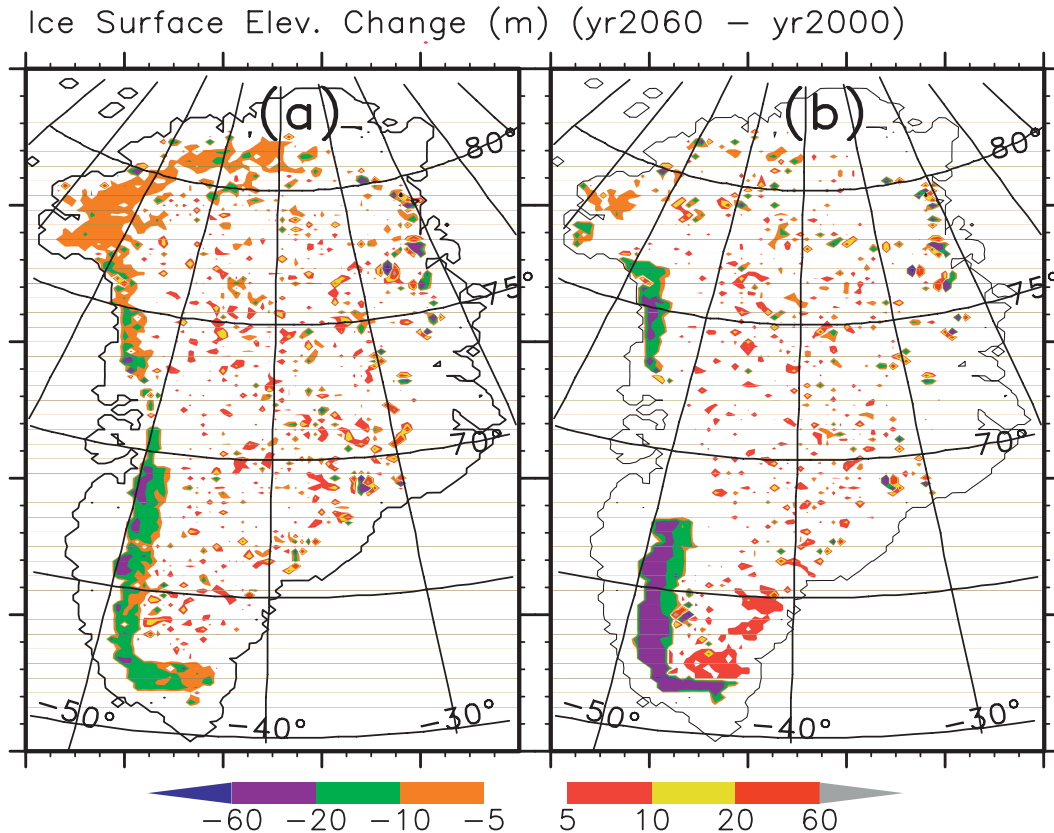

FIG. 7. Surface elevation changes between 2000 and 2060 for (a) CCSM3 and (b) MIROC(hires). The color scales are in meters.
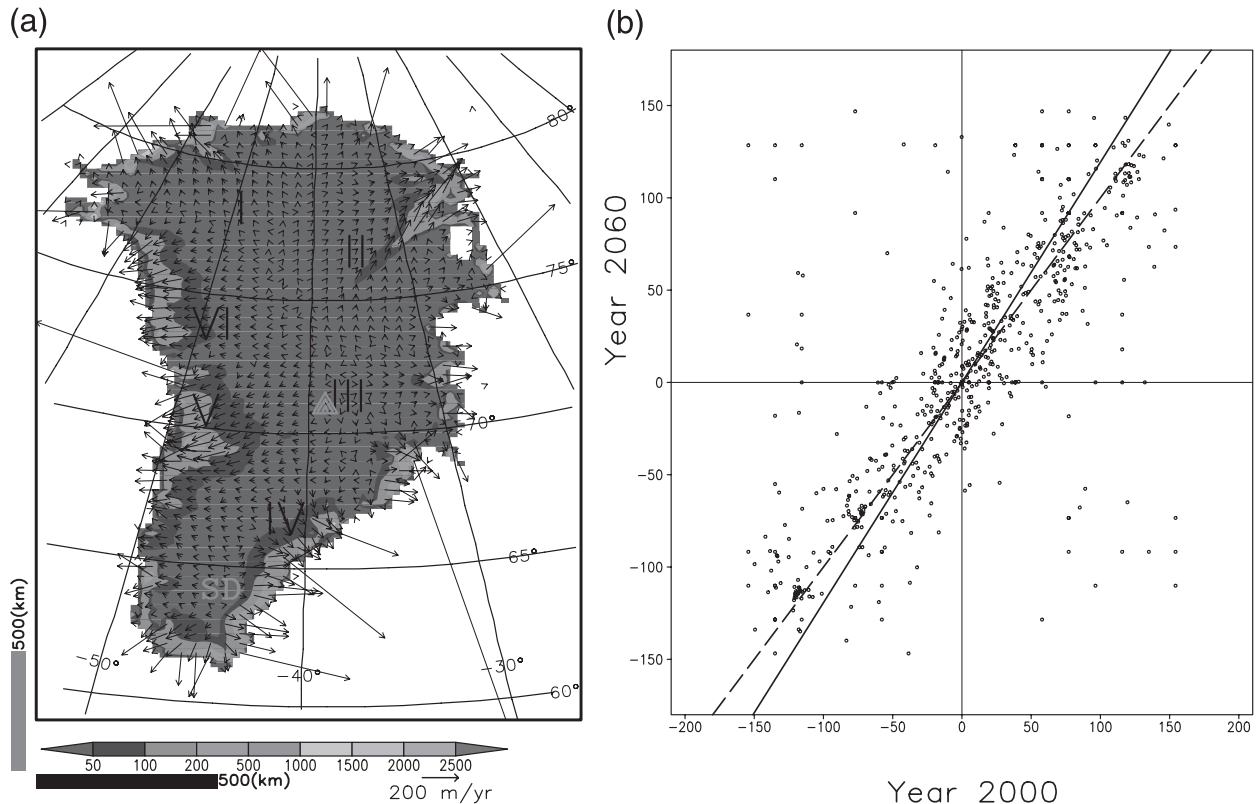
(a)

(b)

FIG. 8. (a) The model-simulated surface velocity field (year 2000), and (b) a scatterplot of the *u* component of velocity, year 2000 (horizontal axis) vs year 2060 (vertical axis).

velocity for grid points above 1500-m elevation for these two years (Fig. 8b). The majority of the flow samples are located in quadrants I and III, suggesting no direction change in ice flow over much of Greenland. The distribution of these samples is along a line with slope 1.09, indicating that the flow magnitudes increase on average by 10% over the next 50 years. More than fifty grid points (~0.4% relative to total grids) are located in quadrants II and IV, suggesting changes in flow direction between 2000 and 2060. Region by region analysis indicate that, by the year 2060, the largest changes in the flow fields are over the northeast (ice divide II) and the southern tip. All ice discharge streams become more concentrated. For ice divide II, the modeled surface velocity at year 2000 reproduces all primary features of the observed surface velocity (Joughin et al. 2001). Examination of the ice surface flow field of year 2060 reveals that, for most of the inland area, the surface flow speed is generally less than 200 m yr^{-1}. However, for drainage divide II, maximum speeds of ~600 m yr^{-1} occur near the grounding lines. A cautionary note is that the ice-flow velocity in the narrow, fast-moving outlets cannot be compared with our model results here because our model spatial resolution is too coarse to resolve the stress discontinuity.

Figure 3 shows the modeled total ice volume change forced by surface climate conditions provided by both CGCMs for the twentieth and twenty-first centuries. The total ice volume obtained from using NCEP–NCAR reanalyses provided atmospheric parameters and GRACE observations, respectively, also is plotted as references for assessing the realism of the changes in total ice volume as determined by the CGCMs. The absolute values are somewhat arbitrary and only the rates of ice volume change are comparable to the observation and that obtained from NCEP–NCAR reanalysis. Both CGCMs underestimate the rate of the total ice volume loss compared to those suggested by GRACE and NCEP–NCAR reanalysis for the period of 2002–08 and 1970–2008, respectively. The projected rates of total ice mass loss also are different between the two CGCMs for the period of 2010–65 with CCSM3 showing no net ice mass loss until 2050. The MIROC3.2(hires) shows a net mass loss rate of ~50 km^3 of ice per year for the period of 2000–50 and reaches ~220 km^3 of ice per year after 2050. The zero or slow rate of total ice mass loss during the first half of the twenty-first century is due mainly to increased precipitation, primarily in the interior of the Greenland, which compensates for the ice mass loss due to increased

melting in the periphery of the ice sheet. Because the ice mass change at this stage is dominated by changes in surface climate conditions, the large discrepancy in the total ice mass loss between the two CGCMs is due to differences in projected climate change, especially change in precipitation, over Greenland. However, after year 2065, both CGCMs project similar rates of rapid ice mass loss because ice flow divergence (enhance by basal sliding and upper surface warming) dominates ice mass loss by the late twenty-first century. Projected surface climate differences from the two CGCMs have a secondary impact on total Greenland ice mass loss.

We further compare total ice volume changes under three different basal conditions (figure not shown): no-slip, the Weertman-type sliding (Weertman 1957, 1983), and granular-type basal sliding using atmospheric parameters projected by CCSM3. The Weertman type of sliding refers to pressure melt at the bottom, for example, the huge overlying weight caused pressure melt at the bottom, whereas the granular-type basal sliding refers to the mechanism as described in MacAyeal (1992). Granular material will be produced by the meltwater erosion on bedrock. The saturated granular material usually is unstably poised on slopes and causing extra basal movement. The effects of basal sliding are small before 2030. Then, as temperatures continue to rise, the basal sliding mechanism becomes significant, especially beneath the southern tip and the northeast ice stream, and signifies a faster mass shed. The differences between the two basal sliding schemes are insignificant prior to 2060. Afterward, the granular basal sliding scheme signifies a far more efficient mechanism for mass shed. Switching between the three constitutive laws (Glen's, Goldsby and Kohlstedt's, and Durham's flow laws) does not change this conclusion. Using the output of the MIROC3.2(hires) as climate forcing gives qualitatively similar results.

It is important to note that as it is a coupled system, the effects of basal sliding do not abruptly "kick in" at a certain time (e.g., at the year 2030). Basal sliding is but one link of a positive feedback chain. Basal sliding is present throughout the simulation and helps warm the ice from inside. Also, it is related to the surface meltwater being channelled into the granular layer (especially in the marginal areas), because granular viscosity is liquid-water-content sensitive (Eq. (3) in Appendix). The total mass balance is a bulk metric. Here just describe the 'general' behavior of the total mass change curve (that after 2030 becomes more noticeably different from that without consideration of basal sliding).

For comparison, we also computed the ice mass loss by the end-of-twenty-first-century carbon emissions for two other emissions scenarios A2 (high) and B1 (low), in addition to the A1B (moderate) scenario. Carbon emissions for these three scenarios range from 5 gigatons of carbon (GtC) yr^{-1} for B1 up to 29 GtC yr^{-1} for A2, with corresponding atmospheric CO_2 concentrations lie between ~500 to ~900 ppmv. The mass loss appears to scale with the atmospheric CO_2 concentration, such that the curve obtained under the A2 scenario shows faster melting than under A1B. Conversely, B1 is a slower melt version than found here. The patterns of geographical change are relatively consistent across all emission scenarios.

For the connected ice regime, no stress discontinuities exist in the ice divides over the entire twenty-first century. Consequently, our simulations show a gradual loss of ice mass in the entire twenty-first century. Our result cannot be used to suggest that the response of the GrIS to climate warming must be gradual in reality.

5. Conclusions

In this study, we investigated the melting of the Greenland ice sheet (GrIS) during the twentieth and twenty-first centuries and the underlying mechanisms, using a new ice dynamics model, SEGMENT-Ice, forced by monthly atmospheric conditions provided by high-resolution climate models. This new ice model is based on the full Navier–Stokes equations that account for nonlocal dynamic balance, and its influence on ice flow and also includes a granular sliding layer between the bottom ice layer and the lithosphere layer to provides a mechanism for large scale surges in a warmer future climate. The monthly climate forcing for this ice sheet model allows an investigation of detailed features such as seasonal melt area extent over Greenland. The model driven by climate conditions from the NCEP–NCAR reanalysis also reproduced reasonably well the annual maximum SME and total ice mass lost rate when compared with those observed by the SSM/I and GRACE.

Simulations of this ice dynamic model are forced by the outputs of the NCAR CCSM3 and MIROC3.2(hires) for the twentieth century "anthropogenic-external forcing" simulations and the twenty-first century simulations under the IPCC moderate emission scenario SRES A1B. The 200-yr simulations allow us to assess impact of anthropogenic-induced warming on mass loss of the GrIS, despite strong decadal and multidecadal natural climate variability. The results suggest that before year 2060 the total mass loss of the GrIS should be relatively slow (~50 km^3 yr^{-1}) and changes of the net balance between the increases of summer surface melting and that of winter precipitation dominate such an ice mass loss. After 2060, the total ice mass loss accelerates rapidly to ~220 km^3 yr^{-1}. The accelerated ice flow and granular basal sliding, due to subsurface positive feedback between

the strain heating and increase of ice flow, becomes dominant and changes in surface climate conditions become less influential. These results highlight the importance of greenhouse gases emissions and temperature increases in the models during the first half of the twenty-first century.

The model results indicate that changes in ice velocity can be forced by changes in subglacial mechanics as well as upper-boundary thermal regime changes, and geometric transitions are governed by changes in flux divergence as well as surface mass balance. This conclusion is especially relevant for a future warming climate.

Calculation of trends is vital in determining whether the observed net mass loss trends continue beyond the survey period. Despite the high climate variability of the high-latitude North Atlantic region, the surveyed melting is attributed primarily to climate warming. Both accumulation and melt rates increase and counteract each other for net mass balance, with an overall negative mass balance. By 2100, the perennial frozen surface area decreases by up to 60%, indicative of a serious expansion of the ablation zone. Ice flow speeds are sensitive to warming. With enhanced surface flow, strain heating increases dramatically and propagates warming effects much deeper than achievable by diffusion alone. Our results show the importance of basal sliding, especially involving granular material, which has been a previously neglected mechanism for fast glacier acceleration and accelerated mass loss. The fact that two independent CGCMs give such similar results adds confidence to our conclusions for longer time scales (>50 years).

APPENDIX

Description of the Ice Sheet Model

This section includes a derivation of the 3D granular rheology law in the context of lithostatic and resistive decomposition, consistent choices for the ice constitutive law and Weertman basal sliding scheme, and the unique treatments of surface melting rate and runoff.

We propose a new ice dynamics model, SEGMENT-Ice, based on the incompressible Navier–Stokes formulation. In standard notations, the mass conservation equation is

$$\nabla \cdot \mathbf{V} = 0 \qquad (A1)$$

and the momentum conservation equation is

$$\rho \left[\frac{\partial \mathbf{V}}{\partial t} + \nabla \cdot (\mathbf{V} \times \mathbf{V}) \right] = \nabla \cdot \boldsymbol{\sigma} + F, \qquad (A2)$$

where ρ is the density, $\mathbf{V}$ is the velocity vector, $\boldsymbol{\sigma}$ is the internal stress tensor, and F is the body force (e.g., gravity $\rho\mathbf{g}$). Instead of using the standard decomposition of the full stress tensor $\boldsymbol{\sigma}$ into static and dynamic stress parts, we decompose it into lithostatic (L) and resistive (R) parts (Van der Veen 1999; Van der Veen and Whillans 1989): $\sigma_{ij} = R_{ij} + \delta_{ij}L$, where R_{ij} denotes the components of the resistive tensor, and δ is the Kronecker operator. This continuum-mechanical formulation is improved further by including acceleration and advection terms for ice motion (Ren et al. 2008).

As a non-Newtonian fluid, polycrystalline ice has a shear-thinning rheology in which the strain-rate is proportional to the applied deviatoric stress raised to an exponent (Glen 1955). This proportionality is temperature dependent (Goldsby and Kohlstedt 2001; Paterson 1994) and follows the parameterization in Hooke (1981). For the Greenland ice domain, this parameterization gives a viscosity range of 4×10^{14}–1.1×10^{15} Pa s. From several possibilities (Goldsby and Kohlstedt 2001), we choose Glen's constitutive relationship because it has proven to be acceptably accurate for studying the large-scale flow characteristics of real glaciers (Van de Veen 1999) and therefore should provide good estimates of total mass loss and overall changes in the surface elevations.

The movement of glacial ice is achieved by a combination of plastic flow, sliding, and the deformation of underlying basal sediments. Pressure-melted water plays an important role in each of these processes. Weertman (1957, 1983) showed how the rate of ice sliding at the local pressure melting temperature (PMP) depends on scales of roughness elements on the glacier bed. However, the

original form of Weertman's law does not fit into the framework of field dimension sliding (Hooke and Iverson 1985), nor does it treat the frictional stresses exerted by entrained sediment particles, which have been identified as important contributors to the overall shear stress at the bed (MacAyeal 1992; Hooke and Iverson 1985). The liquid-like layer separating the ice from the bedrock exists even for glaciers far below the bulk PMP at their beds (Gilpin 1979). This concept has been adopted by modellers and has been observed in the field (Shreve 1984; Hallet 1996). The "grade-glacier" theory (Alley et al. 2003) generalizes silt production and transportation as an integrated component of the ice erosion on glacier bed. It shows that climate fluctuations, by modifying ice surface slope, can affect sediment transport and erosion patterns. This theory directly motivated the present research because the established warming climate may flatten the marginal area of the fast glaciers surrounding the Greenland ice sheet and therefore encourage the deposition of granular sediments.

A Weertman-type sliding law, with overburden pressure corrected for the subglacial water buoyancy, appears well-suited for describing large-scale flow features (see the review in Bindschadler 1983). This makes it appealing to be used together with Glen's law. We follow the treatment of basal sliding coefficient C_b in the SICOPOLIS. The crevasses and moulin distribution (Zwally et al. 2002) may signify an important mechanism for surface meltwater drainage. Owing to a lack of survey data and large uncertainties in their distribution characteristics, it is difficult to directly parameterize their effects on basal sliding. Therefore, we follow an empirical approach, which uses a surface meltwater coefficient, γ, usually between 0 to 6 yr m^{-1}, to enhance C_b, using the linear multiplier $(1 + \gamma m)$, with m being melt rate. The very existence of crevasses is a strong indication of uneven basal erosion, which produces granular material. When Weertman sliding is activated, we separate a granular layer from the bottom bedrock. Unlike ice, the viscosity of granular material depends also on the isotropic stress. For this granular sublayer, a newly proposed rheology (Jop et al. 2006) is applied, namely,

$$\nu = \left(\mu_0 + \frac{\mu_1 - \mu_0}{I_0/I + 1}\right)\frac{S}{|\varepsilon_e|}, \qquad (A3)$$

where ν is viscosity, $S = [R_{kk} - \rho g(h - z)]/3$ is the spherical part of the stress tensor σ, μ_0, and μ_1 are the limiting values for the friction coefficient μ, and μ_1 and μ_0 are liquid water content sensitive. Here, $|\varepsilon_e|$ is the effective strain rate and $|\varepsilon_e| = [0.5(\varepsilon_{ij} \cdot \varepsilon_{ij})]^{0.5}$, I_0 is a constant depending on the local slope of the footing bed as well as the material properties, and I is inertial

number defined as $I = |\varepsilon_e| \, d/(S/\rho_s)^{0.5}$, where d is particle diameter and ρ_s is the particle density. The granular layer thickness, basal material density, and the effective particle size are determined optimally using the datum period. If the retrieved thickness is less than 5 cm, the granular layer is nominal and is not activated. Applying the constitutive relationship reduces the unknowns in Eq. (A2) to the three velocity components (u, v, and w). Based on conservation of mass, momentum and energy, originally nonglaciated grids can be glaciated and vice versa.

We use the following thermal equation (Greve 2005):

$$\rho c\left[\frac{\partial T}{\partial t} + (\mathbf{V} \cdot \mathbf{V})T\right] = k\Delta T + \frac{2}{\nu}\sigma_{\text{eff}}^2, \qquad (A4)$$

where c is heat capacity [(J kg^{-1}) K^{-1}], T is temperature (K), κ is thermal conductivity [W K^{-1}) m^{-1}], and σ_{eff} is effective stress (Pa). The last term is "strain heating" or the converting of work done by gravity into heat used to heat the sliding material or cause phase change.

The dynamic [Eq. (A2)] and thermodynamic [Eq. (A4)] equations are coupled. The upper-boundary condition for Eq. (A2) is that of free stress. The zero-velocity gradient is applied as a lateral boundary condition. The boundary conditions for Eq. (A4) are a surface temperature at top of each grid [$T|_{z=zt} = T_s(x, y)$] and a geothermal flux to the base of the lithosphere layer [$k(\partial T/\partial z)|_{z=zb} = G_0$, here G_0 is geothermal heat flux (W m^{-2})].

The phase change of surface ice is simulated using an energy balance–based melt model (Ren et al. 2007). It takes the surface net radiation and the current state of the surface layer as input. The model then estimates the latent and sensible heat fluxes and budgets the mass within each time step. The ground heat flux is used as an upper-boundary heating/cooling to diagnose the ice temperature. We integrate a prognostic equation that includes full-3D heat advection, internal friction, and heat diffusion to estimate the temperature profile within the ice regime. A semi-implicit temperature solver automatically adjusts iteration time steps within a "big" time step of 24 h. The thinner the layer depth is, the more time consuming is the iteration process. To lessen the computation load, regions with total ice thickness less than 50 m are treated here as a bulk layer for temperature prediction.

For the net mass balance of the ice sheet, arguably the most important quantity is the runoff. We assume a total withholding of the mass for snow falling on the dry snow zone and percolation zone (Benson 1962). Melting water from the ablation zone is assumed to be lost in a manner analogous to water drainage from a porous soil layer. The analogy is between firm and sandy soil. This also applies to other cases involve water redistribution among grids (e.g.,

ponding water and mixed form of precipitation). We use a carefully edited digital mask (referenced to the zones division in Benson 1962) to investigate the refreezing of meltwater and hence to gain improved estimation of the net runoff. Because the form of precipitation under a warming climate may not strictly follow this mask, we assign higher weighting to the surface temperature to determine the precipitation forms. For possible rainfall in the ablation zone, an important mixing process is included [viz., the Q_m term in Eq. (1) of Ren et al. (2007)], because heat transferred to snow by rain during cooling to 0°C is significant (Peng et al. 2002). The GRACE measurements indicate that post glacial rebound (PGR) is not a significant issue within the GrIS range (Fig. 2 in Chen et al. 2006).

REFERENCES

Abdalati, W., and K. Steffen, 2001: Greenland ice sheet melt extent: 1979-1999. *J. Geophys. Res.,* **106** (D24), 33 983–33 989.

Alley, R., 1993: In search of ice-stream sticky spots. *J. Glaciol.,* **39,** 447–454.

——, D. Lawson, G. Larson, E. Evenson, and G. Baker, 2003: Stabilizing feedbacks in glacier-bed erosion. *Nature,* **424,** 758–760.

——, T. Dupont, B. Parizek, S. Anandakrishnan, D. Lawson, G. Larson, and E. Evenson, 2006: Outburst flooding and the initiation of ice-stream surges in response to climatic cooling: A hypothesis. *Geomorpyology,* **75,** 76–89.

Ambach, W., 1985: Characteristics of the Greenland ice sheet for modelling. *J. Glaciol.,* **31,** 3–12.

Bamber, J., S. Ekholm, and W. Krabill, 2001: A new, high-resolution digital elevation model of Greenland fully validated with airborne laser altimeter data. *J. Geophys. Res.,* **106,** 6733–6745.

Benson, C., 1962: Stratigraphic studies in the snow and firn of the Greenland ice sheet. Snow, Ice, and Permafrost Research Establishment Rep. 70, 93 pp.

Bindschadler, R., 1983: The importance of pressurized subglacial water in separation and sliding at the glacier bed. *J. Glaciol.,* **29,** 3–19.

Bromwich, D., Q.-S. Chen, Y. Li, and R. Cullather, 1999: Precipitation over Greenland and its relation to the North Atlantic Oscillation. *J. Geophys. Res.,* **104,** 22 103–22 115.

Chen, J., C. Wilson, and B. Tapley, 2006: Satellite gravity measurements confirm accelerated melting of Greenland ice sheet. *Science,* **313,** 1958–1960.

——, ——, and ——, 2011: Interannual variability of Greenland ice losses from satellite gravimetry. *J. Geophys. Res.,* doi:10.1029/2010JB007789, in press.

Collins, W., and Coauthors, 2007: The community climate system model version 3 (CCSM3). *J. Climate,* **19,** 2122–2143.

Cuffey, K., G. Clow, R. Alley, M. Stuiver, E. Waddington, and R. Saltus, 1995: Large arctic temperature change at the Wisconsin-Holocene glacial transition. *Science,* **270,** 455–458.

Fahnestock, M., R. Bindschadler, R. Kwok, and K. Jezek, 1993: Greenland ice sheet surface properties and ice dynamics from *ERS-1* SAR imagery. *Science,* **262,** 1530–1534.

Genthon, C., 1994: Antarctic climate modeling with general circulation models of the atmosphere. *J. Geophys. Res.,* **99,** 12 953–12 961.

Gilpin, R., 1979: A model of the "liquid-like" layer between ice and a substrate with applications to wire regelation and particle migration. *J. Colloid Interface Sci.,* **68,** 235–251.

Glen, J., 1955: The creep of polycrystalline ice. *Proc. Roy. Soc. London,* **228A,** 519–538.

Goldsby, D. L., 2006: Superplastic flow of ice relevant to glacier and ice-sheet mechanics. *Glacier Science and Environmental Change,* P. G. Knight, Ed., Blackwell, 308–314.

——, and D. Kohlstedt, 2001: Superplastic deformation of ice: Experimental observations. *J. Geophys. Res.,* **106,** 11 017–11 030.

Greve, R., 2000: On the response of the Greenland ice sheet to greenhouse climate change. *J. Climatic Change,* **46,** 289–303.

——, 2005: Relation of measured basal temperatures and the spatial distribution of the geothermal heat flux for the Greenland ice sheet. *Ann. Glaciol.,* **42,** 424–432.

Hallet, B., 1996: Glacial quarrying: A simple theoretical model. *Ann. Glaciol.,* **22,** 1–9.

Hambrey, M., and J. Alean, 2004: *Glaciers.* 2nd ed. Cambridge University Press, 376 pp.

Hasumi, H., and S. Emori, 2004: K-1 coupled GCM (MIROC) description. Center for Climate System Research Tech. Rep. 1, 34 pp. [Available online at http://www.ccsr.u-tokyo.ac.jp/kyosei/hasumi/MIROC/tech-repo.pdf.]

Hegerl, G. C., and Coauthors, 2007: Understanding and attributing climate change. *Climate Change 2007: The Physical Science Basis,* S. Solomon et al., Eds., Cambridge University Press, 663–745.

Hooke, R., 1981: Flow law for polycrystalline ice in glaciers: Comparison of theoretical predictions, laboratory data, and field measurements. *Rev. Geophys. Space Phys.,* **19,** 664–672.

——, and N. Iverson, 1985: Experimental study of ice flow around a bump: Comparison with theory. *Geogr. Ann.,* **67A,** 187–197.

Huybrechts, P., 1994: The present evolution of the Greenland ice-sheet—An assessment by modelling. *Global Planet. Change,* **9,** 39–51.

——, A. Letr'eguilly, and N. Reeh, 1991: The Greenland ice sheet and greenhouse warming. *Global Planet. Change,* **89,** 399–412.

Jop, P., Y. Forterre, and O. Pouliquen, 2006: A constitutive law for dense granular flows. *Nature,* **441,** 727–730.

Joughin, I., M. Fahnestock, D. MacAyeal, J. Bamber, and P. Gogineni, 2001: Observation and analysis of ice flow in the largest Greenland ice stream. *J. Geophys. Res.,* **106,** 34 021–34 034.

Kalnay, E., and Coauthors, 1996: The NCEP/NCAR 40-Year Reanalysis Project. *Bull. Amer. Meteor. Soc.,* **77,** 437–471.

Krabill, W., and Coauthors, 2000: Greenland ice sheet: High-elevation balance and peripheral thinning. *Science,* **289,** 428–430.

Kuhn, M., 1981: Climate and glaciers. Sea Level, Ice, and Glaciers, IAHS Publ. 131, 3–20.

Leslie, L. M., D. J. Karoly, M. Leplastrier, and B. W. Buckley, 2007: Variability of tropical cyclones over the southwest Pacific Ocean using a high-resolution climate model. *Meteor. Atmos. Phys.,* **97,** 171–180, doi:10.1007/S00703-006-0250-3.

MacAyeal, D., 1992: Irregular oscillations of the west Antarctic ice sheet. *Nature,* **359,** 29–32.

Nakicenovic, N., and R. Swart, Eds., 2000: *Special Report on Emissions Scenarios.* Cambridge University Press, 612 pp.

Ohmura, A., M. Wild, and L. Bengtsson, 1996: A possible change in mass balance of Greenland and Antarctica ice sheets in the coming century. *J. Climate,* **9,** 2124–2135.

Paterson, W., 1994: *The Physics of Glaciers.* 3rd ed. Pergamon, 496 pp.

Peng, G., L. M. Leslie, and Y. Shao, 2002: *Environmental Modeling and Prediction.* Springer, 480 pp.

Pollack, H., S. Hurter, and J. Johnson, 1993: Heat flow from the Earth's interior: Analysis of the global data set. *Rev. Geophys.,* **31,** 267–280.

Ren, D., and D. J. Karoly, 2006: Comparison of glacier-inferred temperatures with observations and climate model simulations. *Geophys. Res. Lett.,* **33,** L23710, doi:10.1029/2006GL027856.

——, ——, and L. M. Leslie, 2007: Mountain glacier melting rate for the period 2001–2030 estimated from three CGCM simulations for the Greater Himalayas. *J. Appl. Meteor. Climatol.,* **46,** 890–899.

——, L. M. Leslie, and D. J. Karoly, 2008: Landslide risk analysis using a new constitutive relationship for granular flow. *Earth Interact.,* **12.** [Available online at http://EarthInteractions.org.]

——, R. Fu, L. M. Leslie, R. Dickinson, and X. Xin, 2010: A storm-triggered landslide monitoring and prediction system: Formulation and case study. *Earth Interact.,* **14.** [Available online at http://EarthInteractions.org.]

——, ——, ——, D. J. Karoly, J. Chen, and C. Wilson, 2011: A multirheology ice model: Formulation and application to the Greenland ice sheet, *J. Geophys. Res.,* **116,** D05112, doi: 10.1029/2010JD014855.

Rignot, E., and P. Kanagaratnam, 2006: Changes in the velocity structure of the Greenland ice sheet. *Science,* **311,** 986–990.

——, M. Koppes, and I. Velicogna, 2010: Rapid submarine melting of the calving faces of west Greenland glaciers. *Nat. Geosci.,* **3,** 187–191.

Shreve, R., 1984: Glacier sliding at subfreezing temperatures. *J. Glaciol.,* **30,** 341–347.

Steffen, K., and J. Box, 2001: Surface climatology of the Greenland ice sheet: Greenland climate network 1995-1999. *J. Geophys. Res.,* **106,** 33 951–33 964.

Straneo, F., G. Hamilton, D. Sutherland, L. Stearns, F. Davidson, M. Hammill, G. Stenson, and A. Rosing-Asvid, 2010: Rapid circulation of warm subtropical waters in a major glacial fjord in East Greenland. *Nat. Geosci.,* **3,** 182–186.

Symon, C., L. Arris, and B. Heal, Eds., 2005: *Arctic Climate Impact Assessment.* Cambridge Press, 1042 pp.

Thomas, R., 2001: Program for Arctic Regional Climate Assessment (PARCA): Goals, key findings, and future directions. *J. Geophys. Res.,* **106,** 33 691–33 705.

Van der Veen, C., 1999: *Fundamentals of Glacier Dynamics.* A. A. Balkema, 472 pp.

——, and I. Whillans, 1989: Force budget: I. Theory and numerical methods. *J. Glaciol.,* **35,** 53–60.

van de Wal, R., and J. Oerlemans, 1994: An energy balance model for the Greenland ice sheet. *Global Planet. Change,* **9,** 115–131.

——, and ——, 1997: Modelling the short-term response of the Greenland ice sheet to global warming. *Climate Dyn.,* **13,** 733–744.

Velicogna, I., and J. Wahr, 2006: Acceleration of Greenland ice mass loss in spring 2004. *Nature,* **443,** 329–331.

Wallace, J., 2000: North Atlantic Oscillation/annular mode: Two paradigms—One phenomenon. *Quart. J. Roy. Meteor. Soc.,* **126,** 791–806.

Weertman, J., 1957: On the sliding of glaciers. *J. Glaciol.,* **3,** 33–38.

——, 1983: Creep deformation of ice. *Annu. Rev. Earth Planet. Sci.,* **11,** 215–240.

Weidick, A., 1995: Greenland. *Satellite Image Atlas of Glaciers of the World,* R. S. Williams and J. Ferrigno, Eds., U.S. Geological Survey, 141.

Weng, W., 1995: Untitled. *Arctic,* **48,** 206.

Yin, J., M. Schlesinger, and R. Stouffer, 2009: Model projections of rapid sea-level rise on the northeast coast of the United States. *Nat. Geosci.,* **2,** 262–266.

Zwally, H., and M. Giovinetto, 2001: Balance mass flux and ice velocity across the equilibrium line in drainage systems of Greenland. *J. Geophys. Res.,* **106,** 33 717–33 728.

——, W. Abdalati, T. Herring, K. Larson, J. Saba, and K. Steffen, 2002: Surface melt-induced acceleration of Greenland ice-sheet flow. *Science,* **297,** 218–222.

——, R. Schutz, C. Bentley, J. Bufton, T. Herring, J. Minster, J. Spinhirne, and R. Thomas, cited 2003: GLAS/ICESat L2 Antarctic and Greenland Ice Sheet altimetry data V018, 15 October to 18 November 2003. National Snow and Ice Data Center. [Available online at http://nsidc.org/data/docs/daac/nsidc0304_0305_glas_dems.gd.html.]